



HAL
open science

Apparent stress scaling for tectonic and induced seismicity: Model and observations

Piotr Senatorski

► **To cite this version:**

Piotr Senatorski. Apparent stress scaling for tectonic and induced seismicity: Model and observations. *Physics of the Earth and Planetary Interiors*, 2008, 167 (1-2), pp.98. 10.1016/j.pepi.2008.02.006 . hal-00532137

HAL Id: hal-00532137

<https://hal.science/hal-00532137>

Submitted on 4 Nov 2010

HAL is a multi-disciplinary open access archive for the deposit and dissemination of scientific research documents, whether they are published or not. The documents may come from teaching and research institutions in France or abroad, or from public or private research centers.

L'archive ouverte pluridisciplinaire **HAL**, est destinée au dépôt et à la diffusion de documents scientifiques de niveau recherche, publiés ou non, émanant des établissements d'enseignement et de recherche français ou étrangers, des laboratoires publics ou privés.

Accepted Manuscript

Title: Apparent stress scaling for tectonic and induced seismicity: Model and observations

Author: Piotr Senatorski

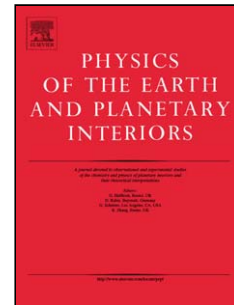
PII: S0031-9201(08)00036-8
DOI: doi:10.1016/j.pepi.2008.02.006
Reference: PEPI 4904

To appear in: *Physics of the Earth and Planetary Interiors*

Received date: 24-9-2007
Revised date: 30-1-2008
Accepted date: 19-2-2008

Please cite this article as: Senatorski, P., Apparent stress scaling for tectonic and induced seismicity: Model and observations, *Physics of the Earth and Planetary Interiors* (2007), doi:10.1016/j.pepi.2008.02.006

This is a PDF file of an unedited manuscript that has been accepted for publication. As a service to our customers we are providing this early version of the manuscript. The manuscript will undergo copyediting, typesetting, and review of the resulting proof before it is published in its final form. Please note that during the production process errors may be discovered which could affect the content, and all legal disclaimers that apply to the journal pertain.



Apparent stress scaling for tectonic and induced seismicity: Model and observations

Piotr Senatorski

*Institute of Geophysics, Polish Academy of Sciences,
ul. Księcia Janusza 64, 01-452 Warsaw, Poland*

Abstract

A macroscopic model of seismic sources provides a scaling relationship for the apparent stress, treated as a function of three independent parameters: seismic moment, rupture area size, and average slip acceleration. These parameters represent three different factors: kinematic, geometric and material. This relationship allows us to distinguish and explain the following statistical characteristics of the log apparent stress versus log seismic moment plot. The regional trends, represented by a series of $1/2$ slope lines, are related to the averaged shape of slip velocity pulses, so they reflect kinematic characteristics of the rupture process. The global trend, represented by the $1/6$ slope line, is expected to characterize sets of events of wide range of rupture area sizes and assumes dependence of rupture area size on total slip, so it is related to the rupture initiation, propagation and arrest conditions; therefore, it reflects earthquake rupture dynamics. Additional shiftings among the trend lines obtained for the smallest induced tremors, larger tectonic earthquakes, and slow tsunami earthquakes, reflect differences between the intact rock failure and the frictional slip failure, that is, between fracture energies of these different earthquake classes.

Key words: Earthquakes, Source parameters, Apparent stress, Seismic energy,

Induced seismicity, Tsunami earthquakes

PACS: 91.30.Bi

1 Introduction

The main objective of macroscopic earthquake physics is to find relations among different earthquake source parameters, such as radiated seismic energy, E_S , seismic moment, M_0 , rupture area size, A , or stress drop, $\Delta\sigma$. All these parameters can be understood as averaged - over the rupture area and duration - characteristics of seismic events. Since parameters of individual earthquakes deviate from any trends or mean values, the relations, if they exist, must represent statistical characteristics of earthquake sets.

Many studies have focused on statistical analysis of earthquake parameters derived from seismograms for earthquake populations. In particular, dependence of the apparent stress, τ_a , expressed as the seismic energy to seismic moment ratio, on the seismic moment has been disputed. The apparent stress value reflects dynamic characteristics of the earthquake rupture processes. Therefore, character of scaling of the apparent stress with earthquake sizes conveys information about mechanisms underlying seismic events. Results of these works are not conclusive. Some data suggest that the apparent stress increases, in the statistical sense, with the increasing seismic moment over a large range of earthquake sizes (e.g., Abercrombie, 1995; Gibowicz, 1997; Izu-tani and Kanamori, 2001; Kanamori and Rivera, 2004; Abercrombie and Rice, 2005; Franceschina et al., 2006). Other data deny that such trends do exist

Email address: psenat@igf.edu.pl (Piotr Senatorski).

(Choy and Boatwright, 1995; McGarr, 1999). According to the more skeptical view, even the observed trends are only artifacts resulting from underestimation of the seismic energy due to the bandwidth limitation effects (Ide and Beroza, 2001).

More reliable estimations of the seismic energy and the apparent stress from seismograms and their proper corrections could help to solve the controversy. The task is not easy, however, because it is not known which of the parameters estimated by seismic or geodetic methods should be chosen as the most adequate set to define seismic sources. Another approach would be to propose a macroscopic model at first, and then to test the postulated relations by using available data.

Such an approach has been proposed in a series of papers. It consists of three steps. In the first step a microscopic model is formulated to describe details of the earthquake rupture process in terms of stress and slip fields defined over a fault plane (Senatorski, 1995; 2002; 2006). The model allows us to express earthquake source parameters as spatial and temporal averages of these fields. In the next step a kinematic model is proposed. It defines an averaged rupture process as a triangle slip velocity pulse propagating along the fault plane. Such a kinematic view, together with expressions for the source parameters implied by the microscopic model, leads to relations among these parameters. In the last step, the macroscopic model is formulated in terms of the macroscopic earthquake source parameters and statistical relations among them (Senatorski, 2005; 2006; 2007).

In particular, the apparent stress, τ_a , has been expressed as a function of three other parameters: M_0 , A , and the average slip acceleration, g . The relation-

ship opens a new perspective for the data analysis. The same data lead to apparently contradicting conclusions, when they are considered in the apparent stress versus seismic moment space, but they do exhibit order, when other parameters, the rupture area size and the average slip acceleration (or, alternatively, the stress drop) are taken into account. Such a new look allows us to recognize two kinds of trends amid the scattered data.

The regional trend concerns sets earthquakes with similar g/A ratio. The data points follow the line with slope ≈ 0.5 in the $\log \tau_a - \log M_0$ space. Its explanation is kinematic and can be related to an average shape of the pulse-like earthquake rupture front (Senatorski, 2006). The global trend concerns earthquakes of all possible spatial sizes. It is represented by the line with a lower slope $\approx 1/6$ in the same space (if there is no systematic change in g). Its explanation takes into account dynamics of the rupture process (Senatorski, 2007). Dependence of the average slip on the rupture area size (so, conditions of initiation, propagation and arrest of the rupture front) is postulated to obtain this trend.

The first aim of the present work is to confront all these theoretical results with more complete sets of available observational data, including not only populations of typical tectonic earthquakes, but also the mining-induced sets of events and slow, tsunami earthquakes. All these sets of data fit well the regional trends described in the previous papers.

The second aim is to present a new result. It might be expected that all the combined data, after rescaling to remove various g/A ratios effect, follow just one trend line with slope ≈ 0.5 . In fact, this is confirmed in the case of typical tectonic earthquakes and larger mining-induced events studied in

the present work. However, the smaller mining-induced tremors do not fit the expected pattern. The trend line (of the same slope ≈ 0.5) is shifted clearly upwards in this case. On the other hand, the trend line of tsunami earthquakes (of the same slope ≈ 0.5) is shifted clearly downwards from the main trend line of typical events. This result seems confusing at first. It occurs, however, that the additional shiftings, or the trend line splitting, can be explained in terms of the stress drop versus slip acceleration relation and differences among fracture energies of these earthquake classes, in accordance with the proposed macroscopic model. With this new result, the whole image remains consistent with observations and earthquake source physics.

The paper is organized as follows. The macroscopic earthquake source model and the scaling relationship for the apparent stress are presented in the next section. Then, the theoretical results are used to analyze the observational data. Interpretation of the proposed scaling relationship and observed trends is presented in the last section. Details of the seismic energy formulation are given in the Appendix.

2 Macroscopic model

The macroscopic model is formulated in terms of relations among earthquake source parameters. It is based on two factors: the microscopic and kinematic model. The microscopic model implies formulation of the seismic energy as a functional of the slip velocity field (see the Appendix). The kinematic model defines such a field as a fixed pulse that propagates along the fault plane. Combination of these two factors leads to the searched relations that are confronted with observational data.

The next sections present such an approach in details. Some of the theoretical results have been presented in the previous paper (Senatorski, 2007). Here, they are repeated, together with new formulas concerning the kinematic model and the slip acceleration versus stress drop relation, to make presentation of the new data analysis (the first aim) and discussion of the trend line splitting (the second aim) complete and clear.

2.1 Slip velocity pulses

The kinematic model is formulated in terms of the slip velocity field, $\dot{q}(t, r)$, defined over the fault plane. It defines an averaged slip velocity pulse by three independent parameters: geometric (size of the rupture area, A), kinematic (rise time, t_R) and material (slip acceleration, g). For simplicity, a planar strike slip fault, with only one, horizontal component of slip and shear stress is assumed.

The triangle slip velocity pulse, same at each point of the rupture area, is assumed (Fig. 1a)

$$\dot{q}(t, r) = g\left(\frac{t_R}{2} - \left|t - \frac{t_R}{2}\right|\right)\chi_{[0, t_R]}(t), \quad (1)$$

where t_R is the pulse rise time, $\chi_{[0, t_R]}$ is the characteristic function on $[0, t_R]$, g - the slip acceleration. Since the averaged rupture process is considered, neither t_R nor g depend on location on the fault plane. The rise time is, in general, shorter than the earthquake duration, $t_R < T$. Other parameters can be expressed in terms of g and t_R . The average coseismic slip displacement at

a given point, D , is

$$D = g \frac{t_R^2}{4}, \quad (2)$$

and the maximum slip velocity, V_m , is

$$V_m = \frac{gt_R}{2}. \quad (3)$$

The local average slip velocity, $V = V_m/2$.

The same slip velocity pulse propagating along the fault plane can be obtained in the following way. Consider the slip displacement function, $q(t = 0, x)$, shown in Fig. 1b

$$q(t = 0, x) = \frac{D}{2a^2} \begin{cases} (x - a)^2 & \text{for } x \in \langle 0, a \rangle \\ -(x + a)^2 + 2a^2 & \text{for } x \in \langle -a, 0 \rangle \end{cases}, \quad (4)$$

The slip displacement at time $t = 0$ decreases from the value $q = D$ (the total slip) at point $x = -a$ to $q = 0$ at point $x = a$. Its movement at velocity V_R produces propagation of the triangle slip velocity pulse $\dot{q}(t, x)$ given by Eq.(1) and shown in Fig. 1a, with the rise time $t_R = 2a/V_R$ and the slip acceleration $g = D(V_R/a)^2$.

The proposed kinematic model seems simplistic. Slip velocity patterns are much more complex than the propagating triangle in real world. However, this model represents the macroscopic approach, so it should be defined by an averaged slip velocity pulse of a given shape (realistic slip and stress patterns have been obtained in computer simulations by using the corresponding microscopic model, e.g., Senatorski, 2002; 2006). Besides, it reproduces essential

characteristics of the rupture process, understood as propagation of a narrow zone of slip movement, driven by stress concentration within and ahead of this zone.

A theory of dislocations can be used to find the shear stress along the slip plane for the slip velocity pulse (1), as the integrated sum of stresses produced by smeared-out infinitesimal dislocations (e.g., Weertman and Weertman, 1980). The stress function, s^I (see the Appendix), obtained for the triangle slip velocity pulse is shown in Fig. 1c. At a given time, $t = 0$, the stress is negative for $x < 0$ and positive for $x > 0$. Its maximum, attained at $x = a/\sqrt{2}$, and minimum, attained at $x = -a/\sqrt{2}$, are proportional to D/a . Also the stress values at $x = \pm a$ (the initial and stopping stresses) are proportional to the D/a value, $s^I(x = \pm a, t = 0) = \pm(\mu \ln 2/\pi)(D/a)$ (numerical values of the initial and maximum stresses are given in Fig. 1c). Far from the slipping zone the stresses tend to zero, $s_I(x \rightarrow \pm\infty, t = 0) = 0$. It can be shown that different shapes of the slip velocity pulse, such as those with $\dot{q} = const$ over the rise time, imply different macroscopic relations than these obtained in the present work, so the model can be falsified.

Another slip time function, parameterized by the maximum slip velocity, V_m , and the rise time, t_R , has been proposed by Beresnev and Atkinson (1997; Beresnev, 2001; 2002). In their approach the seismic source is treated as a point in space observed from the far field. Consequently they find relations between the earthquake source parameters, V_m and t_R , and the point-source acceleration spectrum in the far field characteristics, the corner frequency and the seismic moment. The method of the present work is different. It assumes a spatially extended seismic source and the proposed slip velocity time function is treated as representing the earthquake rupture process which is averaged

over the source area. Consequently statistical relations between mean earthquake characteristics has been found and confronted with trends observed in earthquake populations.

2.2 Seismic moment and energy

The seismic moment is defined as

$$M_0 = \mu \int_T \int_A \dot{q}(t, r) dr dt = \mu DA, \quad (5)$$

where A is the rupture area size, μ is rigidity. The triangle slip velocity pulse (1) substituted into Eq. (5) gives for the seismic moment

$$M_0 = \mu Ag \frac{t_R^2}{4} \quad (6)$$

The seismic energy can be expressed as

$$E_S = \frac{\mu}{2v_S} \int_T \int_A dt dr \dot{q}(r, t)^2. \quad (7)$$

This expression assumes the slip dependent friction and negligible final overshooting. Validity of such an approach is discussed in the Appendix.

The triangle slip velocity pulse (1) substituted into Eq. (7) gives

$$E_S = \frac{\mu}{2v_S} Ag^2 \frac{t_R^3}{12}. \quad (8)$$

2.3 Apparent stress

The apparent stress is expressed as the seismic energy to the seismic moment ratio

$$\tau_a = \mu \frac{E_S}{M_0}. \quad (9)$$

From Eqs. (8) and (9) we obtain

$$\tau_a = \frac{\mu}{2v_S} \frac{\mu}{12M_0} A g^2 t_R^3. \quad (10)$$

The apparent stress can be expressed, from Eqs. (2), (3), (6) and (10), by other parameters as

$$\begin{aligned} \tau_a &= \frac{\mu}{2v_S} g \frac{t_R}{3} = \frac{\mu}{2v_S} \frac{2}{3} (gD)^{1/2} = \frac{\mu}{2v_S} \frac{4}{3} \frac{D}{t_R} \\ &= \frac{\mu}{2v_S} \frac{4}{3} V = \frac{\mu^{1/2}}{3v_S} \frac{g^{1/2} M_0^{1/2}}{A^{1/2}}. \end{aligned} \quad (11)$$

The last equation has been derived previously (e.g., Senatorski, 2006) as the scaling relationship

$$\tau_a(\alpha M_0, \beta A, \gamma g) = \alpha^{1/2} \beta^{-1/2} \gamma^{1/2} \tau_a(M_0, A, g). \quad (12)$$

The slip acceleration, g , rupture area, A , and rise time, t_R , can be changed independently according to the kinematic model. These three parameters fix the model and other earthquake source parameters. The apparent stress, according to Eq. (11), depends on just one parameter, V_m , or any two of three: g , D , and t_R . If the apparent stress versus seismic moment relation is considered, dependence on the rupture area occurs. Therefore, for fixed g/A ratio, τ_a grows as $M_0^{1/2}$. However, events with small and large M_0 can have similar

τ_a , if larger M_0 is due to larger area, A , only, and their total slips, D , are similar. Note that the average slip displacement, its derivatives, and the rise time, has been shown to be basic source parameters that can be derived from seismograms (Beresnev, 2001; 2002).

2.4 Slip acceleration and stress drop

According to the scaling relationship (11) and (12), the apparent stress depends on three factors: kinematic (seismic moment, slip, or rise time), geometric (rupture area or source radius), and material, related to strength of rocks (slip acceleration or rigidity). Unfortunately, the available field data do not contain information about the mean slip accelerations, g . It is assumed, therefore, that the average stress drop, $\Delta\sigma$, scales in the same way as g (if the other independent factors - geometric and kinematic - are fixed) and, therefore, g can be substituted by $\Delta\sigma$ according to the rule:

$$g = \xi^2 \Delta\sigma, \quad (13)$$

where $\xi > 0$ is constant. Consequently, instead of Eq.(11) we can write

$$\tau_a = \frac{\mu^{1/2} \xi \Delta\sigma^{1/2} M_0^{1/2}}{3v_S A^{1/2}}. \quad (14)$$

This assumption can be supported by the following reasoning. Consider the propagating slip displacement shown in Fig.1b. The stress drop, or the difference between the initial (before the pulse passage) and final (after the pulse passage) stress is proportional to D/a value, $\Delta\sigma = (2\mu \ln 2\beta_2/\pi)D/a$, where $\beta_2 = \sqrt{1 - (V_R/v_S)^2}$ (e.g., Weertman and Weertman, 1980). On the other hand, the slip acceleration can be expressed as $g = D(V_R/a)^2$, so it is propor-

tional to the stress drop multiplied by the factor $V_R^2/(a\beta_2)$. Consequently, (13) is justified for constant values of V_R and a . In this case, the slip acceleration, g , changes, but the rise time, t_R , is kept constant.

Another argument supports the assumption. In the microscopic model, the slip velocity at a given point and time is proportional to the net stress (i.e., the driving stress - caused by the tectonic plate movements and slip gradients - minus the stress resisting the fault movement; see Eq.(A.8) in the Appendix; see also Senatorski, 2006). Therefore, it can be assumed that, on an average, the maximal slip velocity of the propagating pulse, V_m , is proportional to $\Delta\sigma$. For the triangle slip velocity pulses, defined by two parameters, g and t_R , $V_m = 2g/t_R$. This means that g scales in the same way with $\Delta\sigma$ as V_m (note that g and t_R are treated as independent parameters; it is assumed that $\Delta\sigma$, or the fault strength, decides about g , not about t_R).

Consequently, both parameters, g and $\Delta\sigma$ can be related to the strength of rocks and, for the purpose of testing, g can be substituted by $\Delta\sigma$ in the scaling relations (11, 12). It should be noticed that both arguments supporting the same scaling for g and $\Delta\sigma$ assume the model used in the present work. The data analysis presented below supports the scaling relationship with $\Delta\sigma$ used instead of g .

An important difference between these two parameters should be noticed. The stress drop represents the difference between the stresses across the fault plane before and after the earthquake. On the other hand, the average slip acceleration (so ξ), unlike $\Delta\sigma$, depends on the entire stress history between these two states and, therefore, carries information about energy expended for fracturing. The same stress drop can lead to small or large slip accelerations

depending on the rate at which the stress resisting the fault movement changes.

The slip dependent friction assumes that fault resistance decreases with increasing slip after its peak value is attained (see the Appendix, Section A.4, and Fig. 5 below). The resistance drops suddenly with slip in the case of fracture of intact rocks. Therefore, the largest g and, consequently, the largest ξ coefficient are expected for the smallest mining-induced tremors, representing this type of the rupture process. On the other hand, the resistance decreases gradually with slip in the case of frictional slip failure, which is representative for larger events. It can be expected, therefore, that g and, consequently, ξ in Eq.(13) are smaller for typical tectonic earthquakes. The smallest ξ coefficient is expected for so called slow or tsunami earthquakes. The same interpretation can be expressed in terms of the energy balance. The fracture energy is represented by the area under resisting (or cohesive) stress line (see the Appendix and Fig. 5). Therefore, smaller ξ corresponds to larger fracture energy. It should be noted that g , not $\Delta\sigma$, remains the basic parameter to be derived from seismograms (cf. Beresnev, 2001; 2002).

2.5 Total slip and rupture area

The kinematic model does not involve any average slip versus rupture area dependence: These two parameters are treated as independent. It is not so, however, that both very small and very large slip velocity pulses could propagate very short and very large distances. Different D versus A scalings have been proposed to explain observations of earthquake populations. For small and moderate events, for instance, the following dependence of slip displacement on earthquake source radius relation is often assumed (e.g., Kanamori

and Anderson, 1975)

$$D = \eta^3 R = \eta^3 A^{1/2}, \quad (15)$$

where $\eta > 0$ is constant. Relations (11) and (15) imply

$$\tau_a = \frac{\mu^{5/6} \eta}{3v_S} g^{1/2} M_0^{1/6}, \quad (16)$$

so $\tau_a \propto M_0^{1/6}$ increase of the apparent stress with increasing seismic moment is expected, provided that there are no systematic variations of g . By using Eq.(13), the same equation can be written as

$$\tau_a = \frac{\mu^{5/6} \eta \xi}{3v_S} \Delta\sigma^{1/2} M_0^{1/6}, \quad (17)$$

so the the same trend is expected for earthquakes representing the same class, i.e., for events with no systematic variations of $\Delta\sigma$ and similar ξ coefficient. Therefore, the smallest mining-induced tremors and the tsunami earthquakes are expected to deviate from the trend line in opposite directions.

It should be noted that relation (15) does not assume any specific source model, but only an intuitive view on the earthquake rupture propagation and arrest condition: The slip velocity pulses characterized by larger slips are expected to cover, on an average, longer distances (e.g., Scholz, 1982; Heaton, 1990; Liu-Zeng et al., 2005). Only large barriers, which are distributed more rarely along the fault plane, can stop pulses with large slip. It is not possible that the pulse with a very small slip (say, 1 cm) cover a distance of 100 km. It can happen, however, that the pulse with quite large slip (say, 1 m) stops after covering a very small distance, if the next stronger barrier is close to the initiation place. A risk of the next larger earthquake increases in such a case.

The relation between the average slip displacement and rupture dimensions (its length and width) for larger earthquakes has been discussed intensively in recent years (e.g., Bodin and Brune, 1996; Mai and Beroza, 2000; Shaw and Scholz, 2001; Liu-Zeng et al., 2005). Details of this problem are beyond the scope of the present paper. Here, the relation (15) is used to show its implications for the apparent stress versus seismic moment scaling. More detailed studies of the slip versus rupture dimension scaling in the context of the apparent stress versus seismic moment relationship can be a subject of future works.

3 Data analysis

Theoretical results presented in previous sections can be compared with observations. Several sets of earthquakes, for which estimations of the seismic energy, E_S , the seismic moment, M_0 , the source radius, $R = \sqrt{A}$, and the average stress drop, $\Delta\sigma$, are available, have been chosen. They are characterized by different mean radii, \bar{R} , from microearthquakes to large events (Table 1). Estimations of all source radii and stress drops assume the source model of Madariaga (1976; see also Gibowicz and Kijko, 1994; Abercrombie and Rice, 2005) with the rupture velocity $V_R = 0.9v_S$. In some cases the original data have been obtained by using the model of Brune (1970); the parameter values have been recalculated in these cases, for consistency, to follow the Madariaga model (see annotations in Table 1). However, results of the present paper do not depend on the choice between the Madariaga or Brune model. Using the RMS stress drop, σ_{rms} , instead of the average stress drop, does not change the results too (see Fig. 2b).

Figures 2, 3 and 4 illustrate trends described by Eqs.(14) and (17). At first, the data are plotted in the $\log \tau_a$ versus $\log M_0$ space (Figs. 2a, 3a, and 4a). It is expected that the apparent stress scales roughly with the seismic moment as $\tau_a \propto M_0^{1/2}$ in the case of sets of earthquakes representing a narrow range of the g/A (or $\xi^2 \Delta\sigma/A$) ratio. Therefore, this kind of statistical dependence is called regional trend in the present work for convenience. Then, the same data are plotted in the $\log \tau_a^*$ versus $\log M_0$ space, where $\tau_a^* = \tau_a \cdot R/\Delta\sigma^{1/2}$ is the scaled apparent stress, to exclude the effect of $\Delta\sigma/A$ ratio variation in earthquake populations (Figs. 2b, 3b, and 4b). The linear dependence $\log \tau_a^* = 0.5 \log M_0 + \log k$ is expected, where $k = \mu^{1/2} \xi / 3v_S$. According to this interpretation the trend line in the scaled apparent stress versus seismic moment space is shifted downwards for earthquake populations having smaller ξ , i.e., larger fracture energy.

Characteristics of the data sets, a number of events, n , ranges of the seismic moments, M_0 , and source radii, R , their mean values, \bar{R} , slopes of the linear regression lines in the $\log \tau_a - \log M_0$ (slope_1) and $\log \tau_a^* - \log M_0$ (slope_2) spaces, together with correlation coefficients, are presented in Table 1.

The following populations of tectonic earthquakes are considered. Moderate earthquakes recorded in the Friuli-Venezia Giulia (Northeastern Italy) area (Franceschina et al., 2006); local microearthquakes recorded in the Granada Basin (Southern Spain) area (Garcia et al., 2004); 4 sets of earthquakes studied by Abercrombie and Rice (2005): events recorded at 2.5 km depth at Cajon Pass, California (Abercrombie; 1995), Northridge aftershocks and Long Valley earthquakes (Mori et al., 2003; Ide et al., 2003), large California earthquakes (Boatwright et al., 2002; Kanamori et al., 1993; McGarr and Fletcher, 2000; Ide et al., 2003; Venkataraman et al., 2000, 2002; Wald and Heaton, 1994;

Dreger and Helmberger, 1991; Mori, 1996; Hough and Dreger, 1995; Wald et al., 1996; Archuleta, 1984; Ji et al., 2002).

Besides, the following sets of mining-induced earthquakes are studied. The smallest tremors induced by excavation of a shaft at Underground Research Laboratory (URL) in Manitoba, Canada (Gibowicz et al., 1991); moderate events induced in Rudna copper mine, Poland (Gibowicz, 2007); events induced in gold mine in South Africa (McGarr, 1994); events induced in mine in Pyhäsalmi, Finland (Oye et al., 2005); events induced in Strathcona mine in Canada (Urbancic and Young, 1993; Urbancic et al., 1996). The URL and Strathcona original data have been corrected to account for the finite bandwidth effects (Di Bona and Rovelli, 1988; Ide and Beroza, 2001).

For comparison, 4 tsunami earthquakes are considered: Peru, 1996, Nicaragua, 1992, Java 1994 (Ihmlé, 1996; Ihmlé et al., 1998; Bilek et al., 2004) and the Sumatra-Andaman 2004 destructive event (Choy and Boatwright, 2007; Sørensen et al., 2007; Banerjee et al., 2007).

Three data sets (Northeastern Italy, Northridge aftershocks and Long Valley) are plotted on separate plots (Figs. 2a,b and 3a,b) to explain details of the data rescaling procedure and the regional trend concept. Then, all data sets are plotted on the same diagrams (Figs. 4a,b) to illustrate trends amid global earthquake data.

3.1 Regional trends

All the data shown in Figs. 2a, 3a, and 4a exhibit, on an average, increase of the apparent stress with increasing seismic moment. However, slopes of the linear

regression lines in the $\log \tau_a - \log M_0$ space are different, from 0.025 to 0.65 (slope_1 column in Table 1). Moreover, the data are largely scattered along the trend lines. For instance, rejection of two points with the largest seismic moments from the Northeastern Italy data set shown in Fig. 2a would result in a steeper trend. According to some authors, the trend observed amid scattered data could be removed by proper measurement correction and rejecting the least reliable data (Ide and Beroza, 2001).

The smallest slope value is obtained, however, for the combined Northridge aftershocks and much smaller Long Valley data (slope_1=0.025, see Fig. 3a). A large difference between mean source diameters of the two earthquake populations is responsible for such a small slope value. For the separate data sets the slope_1 values are larger: 0.17 and 0.21, respectively. Also the set of large earthquakes (slope_1= 0.10) includes three clearly smaller events: one foreshock and two aftershocks; this explains the small value of slope_1 in this case (Fig. 4a).

The scaling relationships (11) and (14) shed light on the problem. After taking into account dependence on two other parameters, the rupture area size and the average slip acceleration (or the stress drop), and after proper rescaling of the apparent stress, the trends become clear (Figs. 2b, 3b, and 4b). Slopes of trend lines tend to the 1/2 value (slope_2 column in Table 1) and the data points focus better along the proper lines. Even the most doubtful data points with the largest seismic moments in Fig. 2 fit well the trend.

Most of these results are in good agreement with the proposed relationship $\tau_a \propto \Delta\sigma^{1/2} M_0^{1/2} / R$. Also the less convincing data, like Northridge aftershocks, are not inconsistent with the trend. For the scaled apparent stress, $\tau_a \cdot R / \Delta\sigma^{1/2}$,

the average slope $\alpha = 0.436$ is obtained for the global data set, with two sets of the smallest tremors (URL and Strathcona mine) and the tsunami earthquakes excluded (Fig. 4b). The excluded data sets fit well the $\tau_a \cdot R / \Delta\sigma^{1/2} - M_0$ scaling, too. However, the trend lines are shifted upwards in the case of the smallest induced events. This means, according to Eq.(14), that ξ is larger for these data sets. Similar effect concerns the tsunami earthquakes, with the trend line shifted downwards. Although estimation of their source diameters and average stress drops are rather rough, it can be suggested, by analogy to the smallest mining-induced tremors, that smaller value of ξ , or larger fracture energy, is responsible for the effect.

3.2 Global trends

Assume that there are no systematic variations of g in the case of earthquakes representing a wide range of rupture area sizes. Then, the averaged (over regional data) apparent stress scales with the seismic moment as $\tau_a \propto M_0^{1/6}$, according to Eq.(16). This global trend is illustrated in Fig. 4a as the slope 1/6 solid line.

Assume then that the factor ξ in Eq.(17) (and, consequently, g) is larger for some data sets. Such a data are shifted upwards in the $\log \tau_a$ versus $\log M_0$ plot. This is the case of two data sets representing the smallest induced tremors (URL and Strathcona). The tsunami events, on the other hand, are characterized by very small apparent stresses. In fact, they are situated well below the data points of large events characterized by similar seismic moments in the Fig. 4a.

The following structure can be recognized in Fig. 4a. Each of the regional

data sets is scattered roughly along the parallel lines (1/2 slope dashed lines), shifted to the right for events having larger rupture area, A (more strictly: smaller g/A ratio; assume for simplicity, however, that there are no systematic variations in g). The data sets representing events with greater A are located higher on the proper 1/2 slope line in such a way that the event characterized by average value of the apparent stress in each of the sets are located along the global trend line (1/6 slope solid line).

3.3 Trend shifting

The mining-induced earthquakes follow the same schema as the tectonic ones. After rescaling, individual data sets fit well the 1/2 slope trends, as shown in Fig. 4b. However, the trend lines found for the smallest tremors are shifted upwards. Moreover, the same data are shifted upwards in Fig. 4a, well above the 1/6 slope global trend line. Both effects can be explained by higher values of the ξ factor in the slip acceleration versus stress drop scaling (13) and, consequently, smaller fracture energy.

This leads us to the following suggestion. The propagating slip velocity pulse shown in Figs. 1a and b, and concentration of stresses ahead of the pulse, describe well general rupture mechanism of both induced and tectonic earthquakes. Linear or piecewise-linear slip velocity changes at a given point are due to the pulse passage. The scaling relation expressed by Eqs. (11) and (12) just reflects this mechanism. Earthquake rupture process on an inhomogeneous fault can be considered, however, as a mixed process between the shear fracture of intact rocks (with sudden decrease of the fault resistance) and frictional slip failure (with gradual decrease of the fault resistance towards

the residual frictional stress level; e.g., Ohnaka, 2003). The smallest induced events are closer to the former process, whereas larger earthquakes are closer to the latter one. It is well known that two types of mining-induced seismicity, related to the intact rock failure and the frictional slip failure, respectively, are observed (e.g., Richardson and Jordan, 2002). It can be expected that, for a given stress drop or rock strength, the slip acceleration is larger in the former case than in the latter one.

Four tsunami earthquakes located in the lower right part of the diagram (Fig.4a) can be considered from the same point of view. The tsunami earthquakes are characterized by exceptionally low seismic energies, in comparison to their seismic moments. Moreover, the data follow the trend line with slope close to $1/2$ (see Table 1 and Fig. 4b). The line is clearly shifted downwards from the main trend line. This is exactly opposite to the smallest tremors case and, therefore, can be explained by low values of the ξ factor in the slip acceleration versus stress drop scaling and larger fracture energy, which is consistent with the fact that such ruptures propagate slowly beneath the accretionary wedge in subduction zones (e.g., Satake and Tanioka, 1999). Since only four tsunami events are considered, the above outlined interpretation needs confirmation by further studies. In particular, the slow earthquake data, characterized by smaller seismic moments, are supposed to follow the same trend line shifted downwards from the main trend line. The whole image is, however, strikingly consistent, so even this small set of slow earthquakes seems to support it.

It is interesting that a similar view - smaller fracture energy for the smallest mining-induced tremors and the largest fracture energy for the tsunami earthquakes - is consistent with estimations of so called radiation efficiency,

$\eta_R = 2\tau_a/\Delta\sigma$, and their interpretation presented in the Appendix.

3.4 Image structure

Each point in the $\log \tau_a$ versus $\log M_0$ plot (Fig. 4a) can be characterized by its $g/A = \text{const}$ line and its position along this line, i.e., the apparent stress value, τ_a . Assume that the material characteristics of the medium (rock strengths, rigidity, slip accelerations, stress drops) exhibit no systematic variation for the studied earthquake populations. For a given g and A (which fix the 1/2 slope line) τ_a depends on the total slip, D , according to Eq.(11). This means that the regional trend is related to the proper g/A value, whereas the global trend is related to D values which are characteristic for given g/A ratios. If the total slip, D , did not depend, on an average, on g/A , the global trend would be represented by a horizontal line.

Thus, the global trend line can be understood as the $D(R)$ dependence. It can be seen that the 1/6 slope line (solid line that crosses the regional stress lines in Fig. 4a), representing the global trend (16), is consistent with most plotted data. The trend assumes that $D \propto R$, as given by Eq.(15).

Most of the data - from microearthquakes to large events - focus along the same slope ≈ 0.5 line in the scaled apparent stress versus seismic moment diagram (Fig. 4b). This means that the apparent stress is proportional to the square root of the slip distance carried by the rupture front pulse, $\tau_a \propto D^{1/2}$, with no systematic variation of rock strengths. Consequently, these events belong to the same class of earthquakes described by the scaling (11) and (12). The smallest induced tremors and the slow tsunami earthquakes belong to two other classes characterized by larger and smaller ξ factor, respectively.

4 Discussion and summary

The kinematic model with the triangle slip velocity pulse propagating along the fault plane implies that the apparent stress depends on three different factors: geometric (represented by the rupture area size, A), kinematic (represented by the total slip, D , the rise time, t_R , or the seismic moment, M_0), and material (represented by the average slip acceleration, g , or the stress drop, $\Delta\sigma$), which can be changed independently. The model leads to the apparent stress scaling which is consistent with the available observational data. The revealed image is as follows (Fig. 4a). For a given data point, the geometric and material factors decide about its regional trend line, i.e., one of a series of slope $1/2$ parallel lines. Lines representing larger g/A are closer to the left edge of the $\log \tau_a - \log M_0$ diagram. Next, the kinematic factor - D , t_R or M_0 - decides about position of the data point along its proper trend line. The data points representing larger total slip, D , are located higher along such a line. The regional trends can be seen clearly in the $\log \tau_a^* - \log M_0$ space, where $\tau_a^* = (A/\Delta\sigma)^{1/2}\tau_a$ (the $g = \xi^2\Delta\sigma$ scaling is used), i.e., after rescaling the apparent stress to take into account the effect of different g/A ratios of individual events (Fig. 4b).

This is not the whole picture, however. The above outlined structure reflects only kinematics of the earthquake rupture process. The next question concerns relation between the total slip D and the rupture area size, A . This problem needs taking into account dynamics of the earthquake rupture process: its initiation, propagation and arrest. A simple assumption that a distance covered by the rupture pulse, or the source diameter, R , is proportional to its characteristic slip displacement, D , leads to another structure in the $\log \tau_a - \log M_0$

diagram: The global trend line with slope $1/6$ (assuming no systematic variations of the material factor, g). Most available data sets are roughly consistent with such a global trend.

The next element of the picture is provided by the induced seismicity and tsunami earthquakes. The smallest tremors are consistent with the scaling relationship suggested by the kinematic model. The rescaled data fit well the expected $1/2$ trend lines in Fig. 4b, they are shifted, however, upwards in the case of the smallest events and downwards in the case of the tsunami earthquakes, from the trend line found for the other data, including larger mining-induced events. The same sets of data are located above or below, respectively, the global trend line in the original $\log \tau_a - \log M_0$ plot (Fig. 4a). Both characteristics can be explained by larger (for the smallest events) or smaller (for the tsunami earthquakes) values of the ξ factor in the $g = \xi^2 \Delta \sigma$ scaling. Since the higher value of ξ is expected to the intact rock failure, or events with smaller fracture energy, the smallest tremors can be related to such a mechanism, with the proposed macroscopic model still valid. Similarly, since the smaller value of ξ is expected to the frictional slip failure, or events with larger fracture energy, the tsunami earthquakes can be related to such a process, with the proposed macroscopic model still valid, too.

The macroscopic model represents averaged view of the earthquake rupture process. It is related to the microscopic earthquake source model formulated in terms of evolution of slip and stress fields over the rupture area (Senatorski, 2002). The link between the two models is the seismic energy formulation (7), which is explained in detail in the Appendix. In the more general form, given by Eq.(A.6) in the Appendix, the seismic energy rate represents the flow out of the ruptured fault plane integrated over the earthquake duration. It assumes

that the slip velocity at a given time and location is proportional to the net stress at the same time and location. Therefore, the static Green function is used in its derivation. Equivalently, friction, not inertia, dominates fault dynamics. It has been argued that this assumption is acceptable in the case of narrow earthquake rupture pulses (e.g., Senatorski, 2002; cf. Ida, 1972). The proposed seismic energy formulation, i.e., the seismic energy rate integrated over the earthquake duration, is strictly valid and consistent with Kostrov's solution (1974) if the rupture process is governed by the slip dependent friction and there is no overshooting. Moreover, it can be shown that the negligible overshoot and interpretation of the trend line shifting in terms of the fracture energy differences are consistent with estimations of the radiation efficiency, $\eta_R = 2\tau_a/\Delta\sigma$, for the studied sets of earthquakes (see the Appendix).

Next assumption of the macroscopic model concerns the triangle (or piecewise-linear) slip velocity pulses (1), illustrated in Fig. 1. It leads, together with the seismic energy formulation (7), to the apparent stress scaling (11, 12). Such a kinematic view is meant as representing the averaged earthquake rupture process, so it must be simplistic. Both observational data analysis and computer simulations, which are based on the microscopic seismic source model in which shapes of the slip velocity pulses are not assumed *a priori* (e.g., Senatorski, 2002; 2006), support this view: Statistical relations between the simulated and real earthquake parameters are consistent with the scaling relations implied by the macroscopic model.

The statistical character of the proposed scaling relationships and trends means that individual data points can deviate from revealed trends or fluctuate around them. This is because of heterogeneity of the rupture process: Parameters of the propagating pulses, such as the rise time or slip acceler-

ation, can variate both in time and space. It has been shown (Senatorski, 2007) that the scaling relationship (12) represents the minimum value of the apparent stress attained for the most uniform rupture process, under the constraints of averaged values the rupture pulse parameters (g, t_R, D, R) , i.e., the process with the same pulses ($t_R < T$) at each point on the fault plane. The absolute minimum is attained for the process which is uniform both in time and in space (the same slip velocity over the whole rupture area and rupture duration, $\dot{q}(t, r) = const, t_R = T$). In the previous papers (Senatorski, 2005; 2006) two questions, interpretation of the apparent stress as a measure of non uniformity of the earthquake rupture process - higher apparent stress means larger non uniformity - and the scaling relationship resulting from the kinematic model, have been treated separately. Interpretation of the scaling in terms of the apparent stress minimalization, under proper constraints, allows us to see these two problems in the same context (Senatorski, 2007).

Summing up the present paper results, three characteristics of the apparent stress versus seismic moment scaling has been recognized and explained within the framework of the proposed model. The regional trend, reflected by $1/2$ slope trend lines in the rescaled log-log apparent stress versus seismic moment plot is due to the rupture process kinematics, or its pulse like style. The global trend, or the $1/6$ slope line in the original log-log apparent stress versus seismic moment plot, reflects the earthquake rupture dynamics, or its nucleation, propagation, and arrest mechanisms. Relative shifting of the regional trend lines for the smallest induced tremors, larger tectonic events, and the tsunami earthquakes, reflects differences between the intact rock failure and the frictional slip failure, or differences of the fracture energy of these three types of seismicity.

Acknowledgements

I thank Jerzy S. Gibowicz for providing corrected mining-induced earthquake data and for stimulating discussions. Constructive or critical reviews by anonymous referees helped me to improve the manuscript.

Accepted Manuscript

A Seismic energy

The seismic energy formulation (7) has been derived previously (e.g., Senatorski, 1994; 1995) by using the overdamped dynamics approximation for the earthquake rupture process governed by the slip dependent friction. This Appendix shows that such a formulation is consistent with the Kostrov's solution (Kostrov, 1974; Kostrov and Das, 1988).

A.1 Model and stress fields

Consider an earthquake source modelled as a vertical cut embedded in an elastic half-space. The earthquake rupture process is represented by evolution of the slip displacement field, $q(r, t)$, defined over the rupture area, A , and the earthquake duration, T . Only horizontal components of slips and shear stresses are considered for simplicity. Distribution of slips before an earthquake, $q_0(r) = q(r, t = 0)$, changes to $q_1(r) = q(r, t = T)$.

Three stress fields contribute to the stress acting at a given point on the fault plane: (a) tectonic or external stress, s^T , due to tectonic plate movements; (b) interaction or internal stress, s^I , due to slip gradients on the fault plane; (c) cohesive and frictional stresses, s^F , that resist the slip movements. A driving stress, s , is defined as a sum of the tectonic and interaction stresses, $s = s^T + s^I$. The net stress is defined as a difference between the driving and resisting stresses, $s - s^F$.

The stress due to interactions can be expressed as a functional of slips, $s^I[q(r, t)]$ (e.g., Okada, 1992; see also Senatorski, 2004). The final stress can be expressed

by the formula:

$$s_1(r) = s^T + \int_A dr' G(r, r') q_0(r') + \int_A dr' G(r, r') D(r') , \quad (\text{A.1})$$

where $G(r, r')$ is the static Green function (note that at $t = 0$ and $t = T$ the system is in equilibrium), and $D(r') = q_1(r') - q_0(r')$ is the final coseismic slip. The first two terms on the right hand side represent the initial stress, $s_0(r) = s(r, t = 0)$, the third one concerns the coseismic change of stress, $s_1(r) - s_0(r)$, where $s_1(r) = s(r, t = T)$.

A.2 Energy balance and seismic energy

The seismic energy can be defined by using the energy balance equation (e.g., Andrews, 1978; Bui, 1978; Rudnicki and Freund, 1981)

$$E_S = -\Delta E_P - (E_G + E_H) , \quad (\text{A.2})$$

where ΔE_P is the potential energy change of the whole system, E_G is the fracture energy, E_H is the frictional energy. It can be represented by slip and stress fields on the fault surface (e.g., Kostrov, 1974; Kostrov and Das, 1988) as

$$E_S = \frac{1}{2} \int_A dr \{s_0(r) + s_1(r)\} D(r) - \int_T dt \int_A dr s^F(r, t) \dot{q}(r, t) , \quad (\text{A.3})$$

where the first term on the right hand side represents the potential energy release, $-\Delta E_P$, and the second one is the energy consumed on the fault surface, $E_G + E_H$. Here, $s_0 = s^T + s^I[q_0(r)]$ is the initial stress, $s_1 = s^T + s^I[q_1(r)]$ is the final stress, in accordance with Eq.(A.1). The original Kostrov's result contains one more term representing loss of mechanical energy at singular fracture edges

($2\gamma_{eff}S$ in Eq.4.4.23, Kostrov and Das, 1988). Due to the assumed cohesive forces acting along the fault surface, however, there are no singularities at the rupture front. Consequently, the fracture energy can be included in the second term on the right hand side of Eq.(A.3) (see also Rudnicki and Freund, 1981; Cocco et al., 2006).

A.3 Supplementary assumptions

Consider the following two assumptions. The overdamped dynamics (assumption 1) allows us to express the driving stress at a given time and location as a functional of slip displacements measured over the entire fault plane at the same time, $s(r, t) = s[q(r, t)]$. The slip-dependent friction (assumption 2) means that the fault resistance to slip movements at a given time and location depends on the slip displacements at the same time and location, $s^F(r, t) = s^F[q(r, t)]$. These two assumptions imply that the net stress at a given time and location on the fault plane, $s - s^F$, can be represented as a functional of slip displacements measured at the same time. They also imply that the evolution equation for the slip displacements can be expressed as a gradient system, $\dot{q} \propto s - s^F = \delta E_S / \delta q$ (Senatorski, 1995; 2004), where the last term denotes the functional derivative of the seismic energy functional, see Eqs. (A.7) and (A.8) below. Although the overdamped dynamics only approximates the full, real dynamics of the process, the seismic energy formulation (A.9) is strictly valid in the case of the slip dependent friction, as shown below.

(1) **Overdamped dynamics:** The stresses are transmitted instantaneously as compared with the slip movements. This implies that the static Green function can be used during the whole rupture history, not only at the initial

and final equilibrium states represented by Eq.(A.1). Therefore, the driving stress, s , that is, the stress due to tectonic forces and slip gradients, can be written as a functional of slip displacements, $s(r, t) = s[q(r, t)]$,

$$s(r, t) = s^T + \int_A dr' G(r, r') q_0(r', t) + \int_A dr' G(r, r') \dot{q}(r', t) . \quad (\text{A.4})$$

(2) **Slip-dependent friction:** At a given point, the cohesive stress function depends on slip displacements only, $s^F(r, t) = s^F[q(r, t)]$. This implies that a time integral in the second term on the right hand side of Eq.(A.3), representing $E_G + E_H$, can be substituted by a slip integral

$$E_G + E_H = \int_T dt \int_A dr s^F[q(r, t)] \dot{q}(r, t) = \int_A dr \int_{q_0}^{q_1} dq s_F[q] . \quad (\text{A.5})$$

According to such a view, a seismic source heterogeneity means that different $s^F[q]$ functions are defined at different points; for instance, they can be characterized by different peak stresses and critical slip displacements, which leads to heterogeneous fault strength distributions. It is also worth noting that the rupture process is defined as evolution of slips and stresses at each point of the fault plane in the present approach, so \dot{q} denotes the partial derivative, $\partial q / \partial t$. Another approach assumes that the cohesive stress zone moves behind a moving crack tip at a rupture velocity V_R . A term proportional to V_R occurs only in the latter approach (see, for instance, Eq.5.3.16 in Freund, 1990).

Assumption 1 implies that Eq.(A.3) can be rewritten as

$$E_S = \int_T dt \int_A dr [s(r, t) - s^F(r, t)] \dot{q}(r, t) . \quad (\text{A.6})$$

In fact, it can be checked that Eq.(A.3) is obtained by substituting Eq.(A.4) into Eq.(A.6).

Assumption 2 allows us to rewrite the seismic energy as the slip integral

$$E_S = \int_A dr \int_{q_0}^{q_1} dq \{s[q] - s^F[q]\} dq . \quad (\text{A.7})$$

Consequently, for given $s_F[q]$, the seismic energy, E_S , depends on initial and final distributions of slips (it does depend on the rupture history through the fault resistance versus slip displacement, $s_F[q]$, dependence). This is an essential property of the slip-dependent friction models.

On the other hand, evolution equations for the slip field can be expressed under the same overdamped dynamics approximation (assumption 1) as (e.g., Senatorski, 1995; cf. Cochard and Madariaga, 1996)

$$\frac{\mu}{2v_S} \dot{q}(r, t) = s(r, t) - s^F(r, t) . \quad (\text{A.8})$$

The right hand side of Eq.(A.8), i.e., the net stress, is a functional of slips in the case of the slip dependent friction (assumption 2). The driving stress at a given point depends on distribution of slips over the entire fault plane, whereas the cohesive stress depends on slips at the same point. In such a case the net stress can be expressed as a functional derivative of the seismic energy function, $\delta E_S / \delta q$, which leads to the seismic energy formulation (A.9) below (see, for instance, Senatorski, 1994; 2004; 2006).

Here, the same final expression for the seismic energy, given also by Eq.(7) in the main text, is obtained from Eqs. (A.6) and (A.8)

$$E_S = \frac{\mu}{2v_S} \int_T \int_A dt dr \dot{q}(r, t)^2 . \quad (\text{A.9})$$

This shows that, in the case of the overdamped dynamics and slip dependent friction model (assumptions 1 and 2) the final expression for the seismic energy

is consistent with the Kostrov's result (A.3).

A.4 Interpretation

Meaning of the evolution equation (A.8) and the energy partition (A.2) is illustrated in Fig. 5, where the stress versus slip (Fig. 5a) and the slip velocity versus slip (Fig. 5b), measured at a given point on the fault plane during three consecutive simulated earthquakes, are shown as an example. The simulations are based on the microscopic earthquake source model (see, for details, Senatorski, 2002; 2006). They were performed for the $100 \times 24 \text{ km}^2$ strike slip fault with strengths (the peak values of the slip dependent cohesive stress) distributed randomly around 6 MPa, with two stronger barriers, and the critical slip distances of 0.6 m distributed uniformly.

The solid line in Fig. 5a is the driving shear stress, s , the area under this line is density of the elastic energy released during rupture, $-\Delta E_P$. The dashed line represents the cohesive stress, s^F , assumed at the measurement point. The fault strength (the peak stress value) is 7.5 MPa at this point. The area under this line represents density of the fracture energy, E_G (the residual frictional stress assumed as zero, so $E_H = 0$). The difference between the two lines is the net stress $(s - s^F) \propto \dot{q}$, or the stress associated with the radiation resistance. The area between the two lines represents density of the seismic energy, E_S , radiated from a given point (see Discussion below).

If the driving stress line follows exactly the cohesive stress line, the stable, quasi-static movement, or slow creeping, takes place at the particular point (the second event shown in Fig. 5); no energy is radiated from this point, $E_S = 0$, during the second event. On the other hand, if the solid line is clearly

above the dashed line, the fast slip movement occur (the third event shown in Fig. 5). In other words, the elastic energy release and the fracture energy are equal, $-\Delta E_P = E_G$, in the quasi-static case.

A.5 Validity

The integrand in Eq.(A.9) represents approximated seismic energy rate function. The dynamics described by Eq.(A.8) ignores inertia or, equivalently, finiteness of the shear wave velocity. However, observations presented in this work seem to support the theoretical results based on this approximation, which needs an explanation.

The first explanation is as follows. It has been heuristically argued that the approximation is justified in the case of narrow slip velocity pulses (e.g., Senatorski, 2002; see also Ida, 1972). Earthquakes seem to exhibit this type of rupture style (e.g., Heaton, 1990; Wald and Heaton, 1994).

This Appendix presents another explanation. Although Eqs.(A.4) and (A.8) describe approximated evolution of slip velocities, driving stresses, and, consequently, seismic energy rate and earthquake rupture history, all based on the static Green function, the seismic energy formulations (A.6) and (A.9) are strictly valid in the case of the slip-dependent friction (assumption 2), provided that final under- and overshooting can be neglected. This is because the seismic energy depends on the initial and final distributions of slips for any assumed functional dependence of frictional and cohesive stresses on slip displacements.

The undershoot or small overshoot have been suggested in the case of tectonic

earthquakes (Smith et al., 1991; Zúñiga, 1993; Hwang et al., 2001). Large overshoot has been suggested in the case the Cajon Pass borehole earthquakes (Beeler et al., 2003). Evidence from laboratory stick-slip friction experiments (Lockner and Okubo, 1983; Okubo and Dieterich, 1984) and observations from mining-induced events (McGarr, 1994) also indicate small or moderate overshoot.

Estimations of the overshoot values use the apparent stress to static stress drop ratio (the Savage-Wood efficiency), $\eta_{SW} = \tau_a/\Delta\sigma$, which is one-half the percentage of the released potential energy that is radiated, or the radiation efficiency, $\eta_R = 2\eta_{SW}$ (see, for instance, Beeler et al., 2003). Analysis based on the energy balance and a simple, uniform, slip-weakening fault model shows that variations of the Savage-Wood efficiency arise both from overshoot, and fracture energy, $\eta_{SW} = 0.5 - \eta^{OV} - \eta^F$, where η^{OV} and η^F denote the stress overshoot and averaged fracture stress (or the cohesive stress), respectively, to the static stress ratio. Note that both the last equation for η_{SW} , and $\Delta\sigma$ estimations are model dependent, so the above mentioned estimations and interpretations should be treated with caution.

It is not clear, which of the two factors, the stress overshoot or the fracture stress, is responsible for deviations of the radiation efficiency from $\eta_R = 1$ value. According to Beeler et al. (2003), for instance, the relatively small mean η_{SW} value for the Cajon Pass events is partially due their large overshoot. Assume, however, that the overshoot (or its variations) can be neglected, and consider changes of η_R for three earthquake classes shown in Fig. 4b. The mean radiation efficiencies for the Strathcona mine tremors (0.84), the Northeastern Italy (0.2) or Cajon Pass events (0.17), and tsunami earthquakes (0.032), illustrate the trend: from the largest values for the smallest tremors to the

smallest values for tsunami earthquakes. Consequently, the smallest fracture energy should characterize the mining-induced tremors, whereas the largest fracture energy should characterize the tsunami earthquakes. This is consistent with the interpretation of the trend line shifting presented in the main text. For the URL tremors $\eta_R = 1.28$, which might suggest the partial stress drop (assuming that both method, and data, are correct). It can be concluded, therefore, that the model with no overshoot is not inconsistent with the present observations. The problem of observational evidence for or against overshooting is open and needs further studies.

A.6 Discussion

The seismic energy representations (A.6) and (A.9) are formulated in terms of the slip velocity and stress fields defined over the fault plane. These two fields can be measured locally, so the integrands in these expressions can be interpreted as the flux of energy radiated out of a given point on the fault surface at a given time. Consequently, the seismic energy can be obtained by summation of the energy flux computed for each point on the fault plane. From Eq.(A.4) it is obvious, however, that both fields, $\dot{q}(r, t)$ and $s(r, t)$, depend on the slip distribution over entire fault plane. Therefore, there is no unique relation between the seismic energy flux measured at a given time and location in the far field, on the one hand, and the flux of energy radiated out of a given point on the fault surface at a given time. Two representations of the seismic energy, the far field and the surface ones, are equivalent; the local energy flux in these two representations, however, are not compatible (cf., Rivera and Kanamori, 2005).

According to some authors, the integrand of the elastic energy release term in Eq.(A.3) has no physical meaning (Rivera and Kanamori, 2005; Fukuyama, 2005). However, Eqs.(A.4) and (A.6) (see also Fig. 5) imply that it represents the driving stress, s , multiplied by the slip velocity, \dot{q} , both measured at a given point on the fault plane, and integrated over earthquake duration, T . The driving stress reflects the rate of decrease of the total energy of the system (elastic energy plus the potential energy of the loading mechanism) approaching equilibrium (e.g., Eshelby, 1956). Consequently it can be defined as a functional derivative of the elastic energy release functional (e.g., Rundle, 1989; Senatorski, 1995).

This interpretation assumes (assumption 1) that the static Green function is used in Eq.(A.4). Thus, the overdamped dynamics approximation, despite its possible limitations, appears to be an effective approach to reveal the structure of the apparent stress versus seismic moment relationship.

References

Abercrombie, R.E., 1995. Earthquake source scaling relationships from -1 to 5 M_L using seismograms recorded at 2.5-km depth, *J. Geophys. Res.* 100, 24015–24036.

Abercrombie, R.E., Rice, J.R., 2005. Can observations of earthquake scaling constrain slip weakening? *Geophys. J. Int.* 162, 406–424, doi:10.1111/j.1365-246X.2005.02579.x.

Andrews, D. J., 1978. Coupling of energy between tectonic processes and earthquakes, *J. Geophys. Res.* 83, 2259–2264.

Archuleta, R.J., 1984. A faulting model for the 1979 Imperial Valley earthquake, *J. Geophys. Res.* 89, 4559–4585.

Banerjee, P., Pollitz, F., Nagarajan, B., Bürgmann, R., 2007. Coseismic slip distributions of the 26 December 2004 Sumatra-Andaman and 28 March 2005 Nias earthquakes from GPS static offsets, *Bull. Seism. Soc. Am.* 97, S86–S102, doi:10.1785/0120050609.

Beeler, N.M., Wong, T.-F., Hickman, S.H., 2003. On the expected relationships among Apparent Stress, static stress drop, effective shear fracture energy, and efficiency, *Bull. Seism. Soc. Am.* 93, 1381–1389.

Beresnev, I., 2001. What we can and cannot learn about earthquake sources from the spectra of seismic waves, *Bull. Seism. Soc. Am.* 91, 397–400.

Beresnev, I., 2002. Source parameters observable from the corner frequency of earthquake spectra, *Bull. Seism. Soc. Am.* 92, 2047–2048.

- Beresnev, I., Atkinson, G., 1997. Modeling finite-fault radiation from the ω^n spectrum, *Bull. Seism. Soc. Am.* 87, 67–84.
- Bilek, S. L., Lay, T., Ruff, L. J., 2004. Radiated seismic energy and earthquake source duration variations from teleseismic source time functions for shallow subduction zone thrust earthquakes, *J. Geophys. Res.* 109, doi:10.1029/2004JB003039.
- Boatwright, J., Choy, G.L., Seekins, L.C., 2002. Regional estimates of radiated seismic energy, *Bull. seism. Soc. Am.* 92, 1241–1255.
- Bodin, P., Brune, J.N., 1996. On the scaling of slip with rupture length for shallow strike-slip earthquakes: quasi-static models and dynamic rupture propagation, *Bull. Seism. Soc. Am.* 86, 1292–1299.
- Brune, J.N., 1970. Tectonic stress and the spectra of seismic shear waves from earthquakes, *J. Geophys. Res.* 75, 4997–5009.
- Bui, H.D., 1978. *Mécanique de la rupture fragile* Masson, Paris-New York-Barcelona-Milan.
- Choy, L.G., Boatwright, J.L., 1995. Global patterns of radiated seismic energy and apparent stress, *J. Geophys. Res.* 100, 18205–18228.
- Choy, L.G., Boatwright, J.L., 2007. The energy radiated by the 26 December 2004 Sumatra-Andaman earthquake estimated from the 10-Minute P-wave windows, *Bull. Seism. Soc. Am.* 97, S18–S24, doi:10.1785/0120050623.
- Cocco, M., Spudich, P., Tinti, E., 2006. On the mechanical work absorbed on faults during earthquake ruptures, in *Earthquakes: Radiated energy and the physics of faulting*. Abercrombie, R., McGarr, A., Kanamori, H., DiToro, G. (Eds.), AGU Geophys. Monogr. Ser., Vol. 170, American Geophysical Union,

Washington D.C., pp.237–254.

Cochard, A., Madariaga, R., 1996. Complexity of seismicity due to highly rate-dependent friction, *J. Geophys. Res.* 101, 25321-25336.

Di Bona, M., Rovelli, A., 1988. Effects of the bandwidth limitation on stress drops estimated from integrals of the ground motion, *Bull. Seism. Soc. Am.* 78, 1818–1825.

Dreger, D., Helmberger, D., 1991. Source parameters of the Sierra Madre earthquake from regional and local body waves, *Geophys. Res. Lett.* 18, 2015–2018.

Eshelby, J.D., 1956. The continuum theory of lattice defects, *Solid State Physics* 3, 79–144.

Franceschina, G., Kravanja S., Bressan G., 2006. Source parameters and scaling relationships in the Friuli-Venezia Giulia (Northeastern Italy) region, *Phys. Earth Planet. Interiors* 154, 148–167.

Freund, L.B., 1990. *Dynamic fracture mechanics*, Cambridge Monographs on Mechanics and Applied Mathematics, Cambridge University Press, Cambridge.

Fukuyama, E., 2005. Radiation energy measured at earthquake source, *Geophys. Res. Lett.* 32, L13308, doi:10.1029/2005GL022698.

Garcia Garcia, J.M., Romacho M.D., Jimenéz A., 2004. Determination of near-surface attenuation, with κ parameter, to obtain the seismic moment, stress drop, source dimension and seismic energy for microearthquakes in the Granada Basin (Southern Spain), *Phys. Earth Planet. Interiors* 141, 9–26.

Gibowicz, S.J., 1997. Scaling relations for seismic events at Polish copper mines, *Acta Geophys.Pol.* 45, 169–181.

Gibowicz, S.J., 2007. Internal report, Inst. of Geophys. PAS (unpublished).

Gibowicz, J.S., Kijko, A., 1994. An introduction to Mining Seismology, Academic Press, San Diego, CA.

Gibowicz, S.J., Young, R.P., Talebi, S., Rawlence, D.J., 1991. Source parameters of seismic events at the underground research laboratory in Manitoba, Canada: Scaling relations for events with moment magnitude smaller than -2, *Bull. Seism. Soc. Am.* 81, 1157–1182.

Heaton, T.H., 1990. Evidence for an implications of self-healing pulses of slip in earthquake rupture, *Phys. Earth Planet. Interiors* 64, 1–20.

Hough, S.E., Dreger, D., 1995. Source parameters of the 23 April 1992 M 6.1 Joshua Tree, California, earthquake and its aftershocks ; empirical Green's function analysis of GEOS and TERRAscope data, *Bull. Seism. Soc. Am.* 85, 1576–1590.

Hwang, R.-D., Wang, J.-H., Huang, B.-S., Chen, K.-C., Huang W.-G., Chang T.-M., Chiu, H.-C., Tsai, C.-C.P., 2001. Estimates of stress drop of the Chi-Chi, Taiwan, earthquake of 20 September 1999 from near field seismograms, *Bull. Seism. Soc. Am.* 91, 1158–1166.

Ida, Y., 1972. Cohesive force across the tip of a longitudinal-shear crack and Griffith's specific energy, *J. Geophys. Res.* 77, 3796-3805.

Ide, S., Beroza, G.C., 2001. Does apparent stress vary with earthquake size? *Geophys. Res. Lett.* 28, 3349–3352.

Ide, S., Beroza, G.C., Prejean, S.G., Ellsworth, W.L., 2003. Apparent break in earthquake scaling due to path and site effects on deep borehole recordings, *J. Geophys. Res.* 108, 10.1029/2001JB001617.

Ihmlé, P.F., 1996. Monte Carlo slip inversion in the frequency domain: Application to the 1992 Nicaragua slow earthquake, *Geophys. Res. Lett.* 23, 913-916.

Ihmlé, P.F., Gomez, J-M., Heinrich, P., Guibourg, S., 1998. The 1996 Peru tsunamigenic earthquake: Broadband source process, *Geophys. Res. Lett.* 25, 2691-2694.

Izutani, Y., Kanamori, H., 2001. Scale dependence of seismic energy-to-moment ratio for strike-slip earthquakes in Japan, *Geophys. Res. Lett.* 28, 4007-4010.

Ji, C., Wald, D.J., Helmberger, D.V., 2002. Source description of the 1999 Hector Mine, California. Part II: Complexity of slip history, *Bull. Seism. Soc. Am.* 92, 1208-1226.

Kanamori, H., Anderson, D.L., 1975. Theoretical basis of some empirical relations in seismology, *Bull. Seism. Soc. Am.* 65, 1073-1095.

Kanamori, H., Mori, J., Hauksson, E., Heaton, T.H., Hutton, L.K. and Jones, M.L., 1993. Determination of earthquake energy release and M_L using terrascoppe, *Bull. Seism. Soc. Am.* 81, 330-346.

Kanamori, H., Rivera, L., 2004. Static and dynamic scaling relations for earthquakes and their implications for rupture speed and stress drop, *Bull. Seism. Soc. Am.* 94, 314-319.

Kostrov, B.V., 1974. Seismic moment and energy of earthquakes and seismic flow of rock. *Izv. Phys. Solid Earth* 13, 13-21.

Kostrov, B.V., Das, S., 1988. Principles of earthquake source mechanics, Cambridge Monographs on Mechanics and Applied Mathematics, Cambridge University Press, Cambridge, New York.

Liu-Zeng, J., Heaton, T., DiCaprio, Ch., 2005. The effect of slip variability on earthquake slip-length scaling. *Geophys. J. Int.* 162, 841–849, doi:10.1111/j.1365-246X.2005.02679.x.

Lockner, D.A., Okubo, P.G., 1983. Measurements of frictional heating in granite, *J. Geophys. Res.* 88, 4313–4320.

Madariaga, R., 1976. Dynamics of an expanding circular fault, *Bull. Seism. Soc. Am.* 66, 639–666.

Mai, P.M., Beroza, G.C., 2000. Source scaling properties from finite-fault-rupture models, *Bull. Seism. Soc. Am.* 90, 604–615.

McGarr, A., 1994. Some comparisons between mining-induced and laboratory earthquakes. *Pure Appl. Geophys.* 142, 467–489.

McGarr, A., 1999. On relating apparent stress to the stress causing earthquake fault slip. *J. Geophys. Res.* 104, 3003–3011.

McGarr, A., Fletcher, 2000. A method for mapping apparent stress and energy radiation applied to the Northridge earthquake fault zone, *Geophys. Res. Lett.* 27, 1953–1956.

Mori, J., 1996. Rupture directivity and slip distribution of the M4.3 foreshock to the 1992 Joshua Tree earthquake, southern California, *Bull. Seism. Soc. Am.* 86, 805–810.

Mori, J., Abercrombie, R.E., Kanamori, H., 2003. Stress drop and radiated en-

ergies of the Northridge aftershocks, *J. Geophys. Res.* 108, 2545, 10.1029/2000JB000474.

Ohnaka, M., 2003. A constitutive scaling law and a unified comprehension for frictional slip failure, shear fracture of intact rock, and earthquake rupture. *J. Geophys. Res.* 108(B2), 2080, doi: 10.1029/2000JB000123, ESE 6-1.

Okada, Y., 1992. Internal deformation due to shear and tensile faults in the half-space, *Bull. Seism. Soc. Am.* 82, 1018–1040.

Okubo, P.G., Dieterich, J.H., 1984. Effects of physical fault properties on frictional instabilities produced on simulated faults, *J. Geophys. Res.* 89, 5817–5827.

Oye, V., Bungum, H., Roth, M., 2005. Source parameters and scaling relations of mining related seismicity within the Pyhäsalmi ore mine, Finland, *Bull. Seism. Soc. Am.* 95, 1011–1026, doi:10.1785/0120040170.

Richardson, E., Jordan, T.H., 2002. Seismicity in deep gold mines in South Africa: Implications for tectonic earthquakes, *Bull. Seism. Soc. Am.* 92, 1766–1782.

Rivera, L., Kanamori, H., 2005. Representations of the radiated energy in earthquakes. *Geophys. J. Int.* 162, 148–155, doi:10.1111/j.1365-246X.2005.02648.x.

Rudnicki, J.W., Freund, L.B., 1981. On energy radiation from seismic sources, *Bull. Seism. Soc. Am.* 71, 583–595.

Rundle, J.B., 1989. A physical model for earthquakes: 3. Thermodynamical approach and its relation to nonclassical theories of nucleation, *J. Geophys. Res.* 94, 2839–2855.

Satake, K., Tanioka, Y., 1999. Sources of tsunami and tsunamigenic earth-

quakes in subduction zones. *Pure Appl. Geophys.* 154, 467-483.

Scholz, Ch.H., 1982. Scaling laws for large earthquakes: Consequences for physical models, *Bull. Seism. Soc. Am.* 72, 805–810.

Senatorski, P., 1994. Spatio-temporal evolution of faults: deterministic model, *Physica D* 76, 420–435.

Senatorski, P., 1995. Dynamics of a zone of four parallel faults: A deterministic model, *J. Geophys. Res.* 100, 24111–24120.

Senatorski, P., 2002. Slip-weakening and interactive dynamics of an heterogeneous seismic source, *Tectonophysics* 344, 37–60.

Senatorski, P., 2004. Interactive dynamics of a heterogeneous seismic source: A model with the slip-dependent friction, *Publ. Inst. Geophys. Pol. Acad. Sci. A-27*, 354, pp.151.

Senatorski, P., 2005. A macroscopic approach towards earthquake physics: the meaning of the apparent stress, *Physica A* 358, 551–574.

Senatorski, P., 2006. Fluctuations, trends, and scaling of the energy radiated by heterogeneous seismic sources. *Geophys. J. Int.* 166, 267–276, doi:10.1111/j.1365-246X.2006.02942.x.

Senatorski, P., 2007. Apparent stress scaling and statistical trends, *Phys. Earth planet. Interiors* 160, 230–244.

Shaw, B.E., Scholz, Ch.H., 2001. Slip-length scaling in large earthquakes: Observations and theory and implications for earthquake physics, *Geophys. Res. Lett.* 28, 1–14.

Smith, K.D., Brune, J.N., Priestley, K.F., 1991. The seismic spectrum, radiated energy, and Savage and Wood inequality for complex earthquakes, *Tectonophysics* 188, 303–320.

Sørensen, M.B., Atakan, K., Pulido, N., 2007. Simulated strong ground motions for great M9.3 Sumatra-Andaman earthquake of 26 December 2004, *Bull. Seism. Soc. Am.* 97, S139–S151, doi:10.1785/0120050608.

Urbancic, T.I., Young, R.P., 1993. Space-time variations in source parameters of mining-induced seismic events with $M \geq 0$, *Bull. Seism. Soc. Am.* 83, 378–397.

Urbancic, T.I., Trifu, C.-I., Mercer, R.A., Feustel, A.J., Alexander, J.A.G., 1996. Automatic time-domain calculation of source parameters for analysis of induced seismicity, *Bull. Seism. Soc. Am.* 86, 1627–1633.

Venkataraman, A., Mori, J., Kanamori, H., Zhy, L., 2000. Fine structure of the rupture zone of the April 26 and 27, 1997, Northridge aftershocks, *J. Geophys. Res.* 105, 19085–19093.

Venkataraman, A., Rivera L., Kanamori, H., 2002. Radiated energy from the 16 October 1999 Hector Mine earthquake: regional and teleseismic estimates, *Bull. Seism. Soc. Am.* 92, 1256–1265.

Wald, D.J., Heaton, T.H., 1994. Spatial and temporal distribution of slip for the 1992 Landers, California, earthquake, *Bull. Seism. Soc. Am.* 84, 668–691.

Wald, D.J., Heaton, T.H., Hudnut, K.W., 1996. The slip history of the 1994 Northridge, California, earthquake determined from strong-motion, teleseismic, GPS, and leveling data, *Bull. Seism. Soc. Am.* 86 (1, Part B Suppl.), 49–70.

Weertman, J., Weertman, J.R., 1980. Moving dislocations, in Dislocations in solids, v.3. Nabarro, F.R.N. (Ed.), North Holland Publ. Comp., Amsterdam-New York, pp.1-59.

Zúñiga, F.R., 1993. Frictional overshoot and partial stress drop. Which one? Bull. Seism. Soc. Am. 83, 939–944.

Accepted Manuscript

FIGURE CAPTIONS

Figure 1. (a) The triangle slip velocity pulse, measured at a given point $P(x = a)$, assumed in the kinematic model; t_R is the rise time, V_m is the maximum slip velocity. The slip acceleration $g = 2V_m/t_R$. (b) The slip displacement function $q(t, x)$; at time $t = 0$ it decreases from $q = D$ (the total slip) at $x = -a$ to $q = 0$ at $x = a$; its movement at velocity V_R produces propagation of the triangle slip velocity pulse shown in (Fig. 1a), with the rise time $t_R = 2a/V_R$ and the slip acceleration $g = D(V_R/a)^2$. (c) The shear stress caused by propagation of the slip displacement along the fault plane; the stress drop, or the difference between the initial (before the pulse passage) and final (after the pulse passage) stress is proportional to D/a (the "relativistic" factor β_2 - see the main text - is ignored in the diagram).

Figure 2. (a) The $\log \tau_a$ as a function of $\log M_0$ for the set of 53 small and moderate earthquakes recorded in the Friuli-Venezia Giulia (Northeastern Italy) area (Franceschina et al., 2006), with source radii ranging from 0.1 to 2.7 km (with mean value 0.42 km). The slope of the linear regression line is 0.30. (b) The $\log \tau_a R / \Delta \sigma^{1/2}$ as a function of $\log M_0$ for the same set of earthquakes. The slope of the linear regression line is 0.42. For comparison, the RMS stress drop is used instead the average stress drop (slope 0.44).

Figure 3. (a) The $\log \tau_a$ as a function of $\log M_0$ for the set of 29 Northridge aftershocks, with source radii ranging from 0.492 to 2.544 km (with mean value 0.864 km) and 14 Long Valley events (Abercrombie and Rice, 2005), with source radii ranging from 0.014 to 0.089 km (with mean value 0.042 km). The slopes of the linear regression lines for these two data sets are 0.17 and

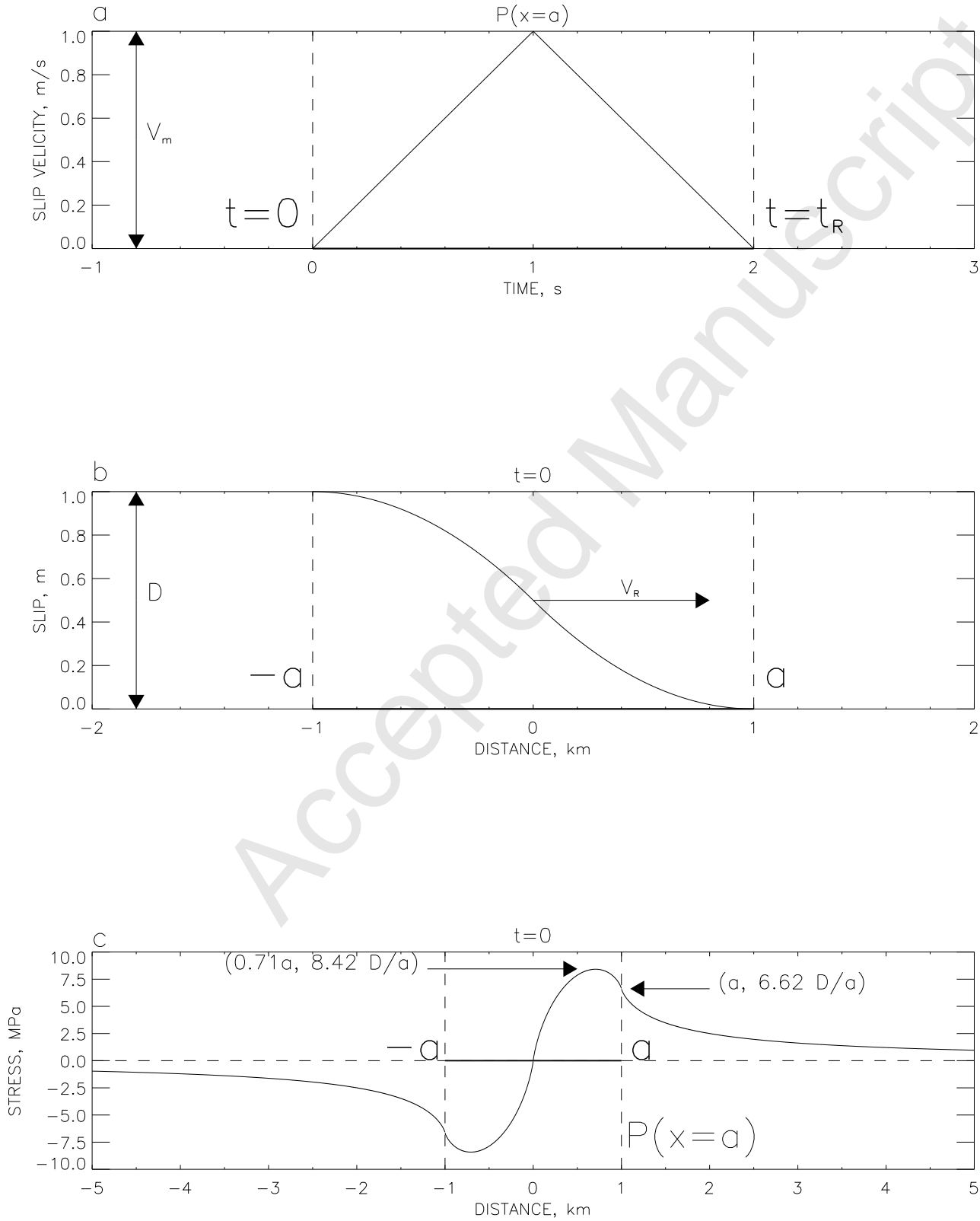
0.21, respectively. The slope for combined all plotted data is 0.025. (b) The $\log \tau_a R / \Delta \sigma^{1/2}$ as a function of $\log M_0$ for the same set of earthquakes. The slopes of the linear regression line are, respectively, 0.21, 0.34, and 0.33, respectively.

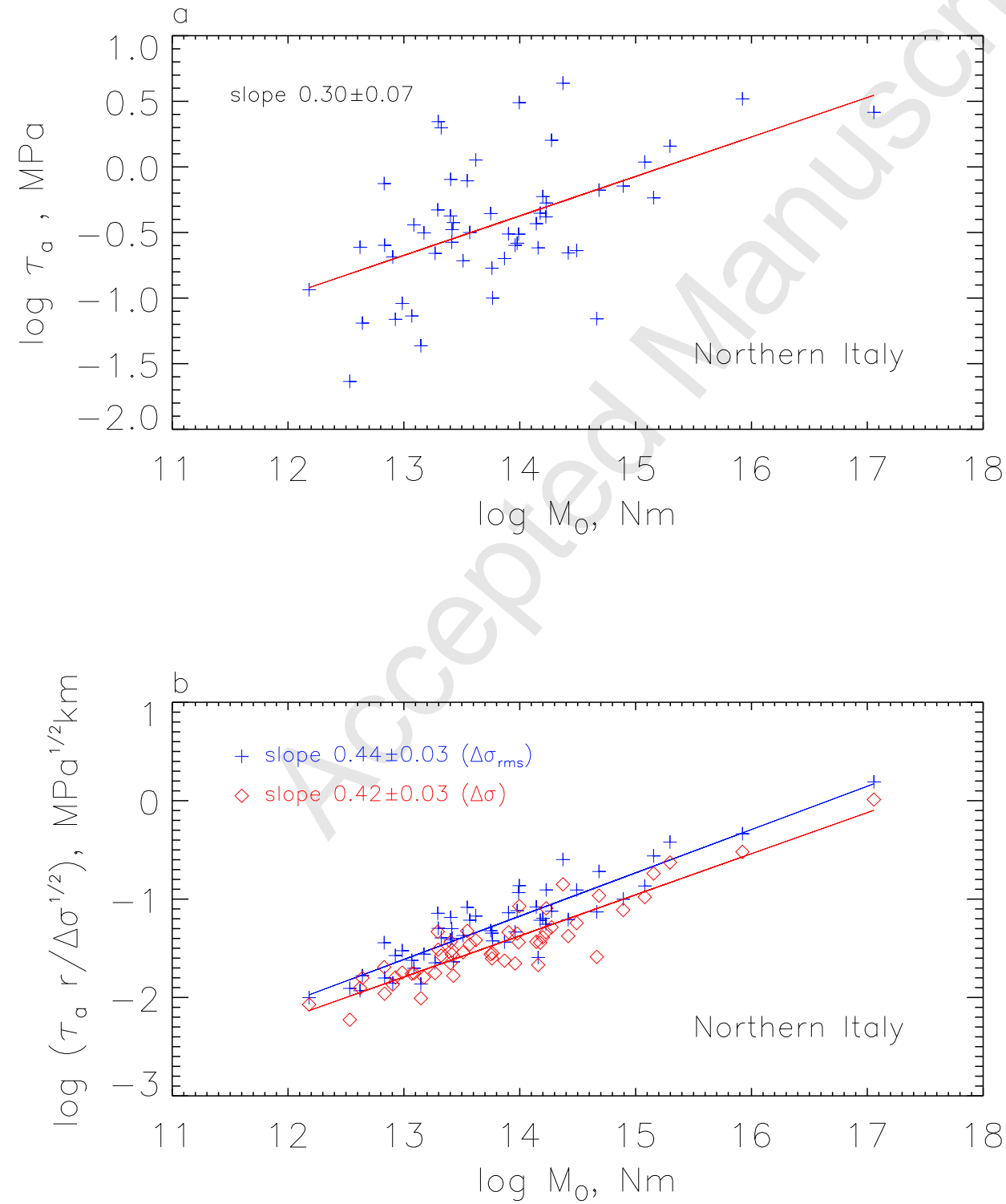
Figure 4. (a) Illustration of the scaling relationship for the apparent stress, τ_a , as a function of the seismic moment, M_0 , the rupture area A , and the average slip acceleration g . A series of lines with slope 1/2 of constant g/A (increasing in the left direction) represents the regional trends. The solid line with slope 1/6 represents the global trend. The following earthquake data are shown: dotted circles - the smallest induced tremors ($R \approx 1$ m, Gibowicz et al., 1991), times signs - Strathcona mine earthquakes (Urbancic and Young, 1993; Urbancic et al., 2005), triangles - Pyhäsalmi mine earthquakes (Oye et al., 2005), asterisks - Rudna mine earthquakes (Gibowicz, 2007), plus signs - South Africa mine earthquakes (McGarr, 1994), circles with plus signs - Cajon Pass earthquakes (Abercrombie, 1995; Abercrombie and Rice, 2005), diamonds - microearthquakes (Spain; Garcia et al., 2004), squares - small and moderate earthquakes (Italy; Franceschina et al., 2006), diamonds with plus signs - Northridge aftershocks and Long Valley events (from Abercrombie and Rice, 2005); filled diamonds - large earthquakes, California (from Abercrombie and Rice, 2005), filled circles - four tsunami earthquakes (P-Peru 1996, Ni-Nicaragua 1992, J-Java 1994; SA-Sumatra Andaman, 2004; different sources). (b) The scaled apparent stress, $\log \tau_a R / \Delta \sigma^{1/2}$ as a function of $\log M_0$ for chosen sets of earthquakes shown in Fig. 4a. The slope of the linear regression line is 0.436. The data points of the smallest tremors and the tsunami earthquakes are shifted upwards and downwards, respectively.

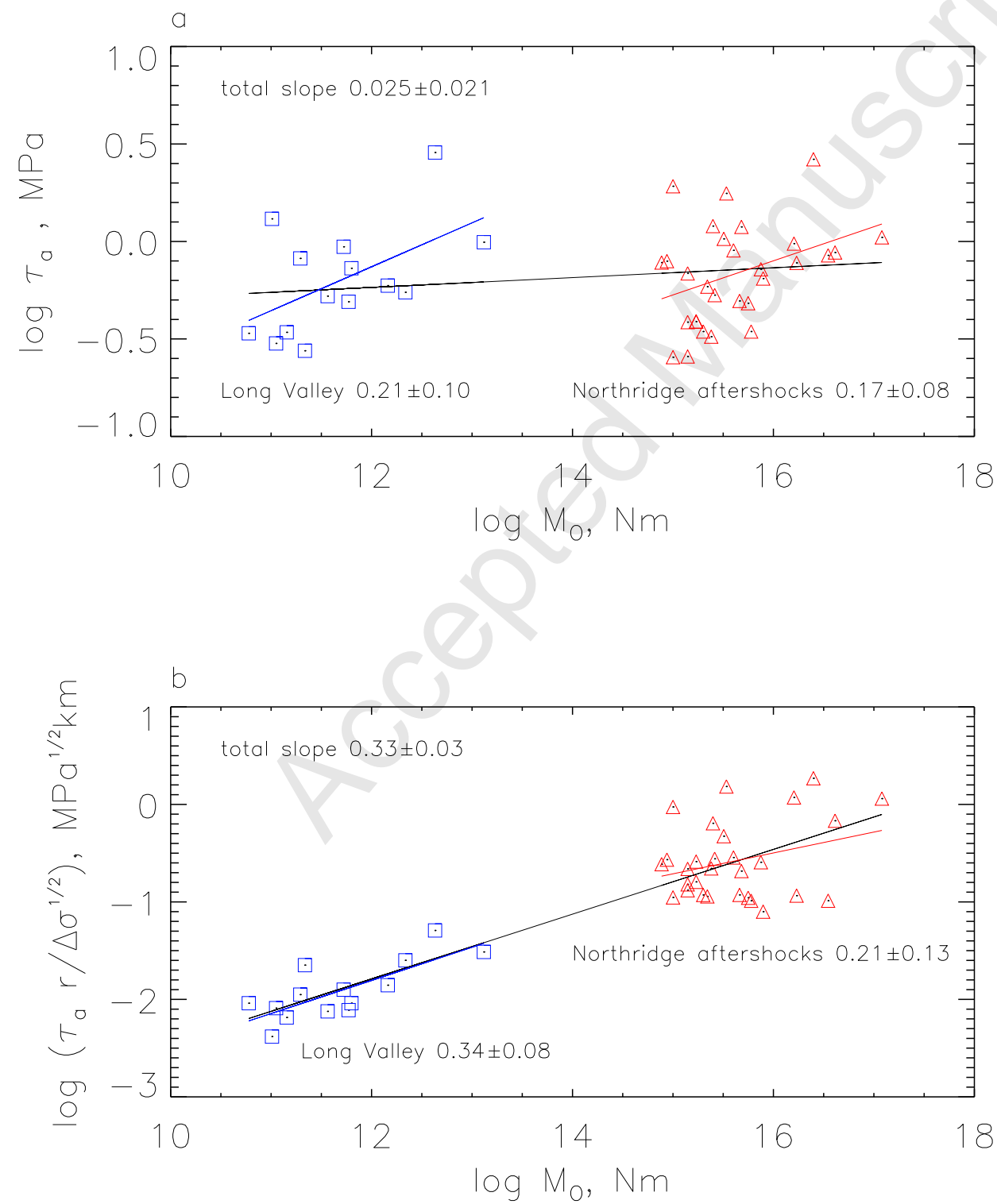
Figure 5. Illustration of stress and slip velocity variations at a given point during consecutive simulated earthquakes. (a) Driving (solid line) and cohesive (dotted line) stresses as functions of slip displacements; (b) slip velocity measured at the same point. The slip velocity is proportional to the difference between the driving and cohesive stress. The area between the driving and cohesive stress lines represents density of energy radiated from this point.

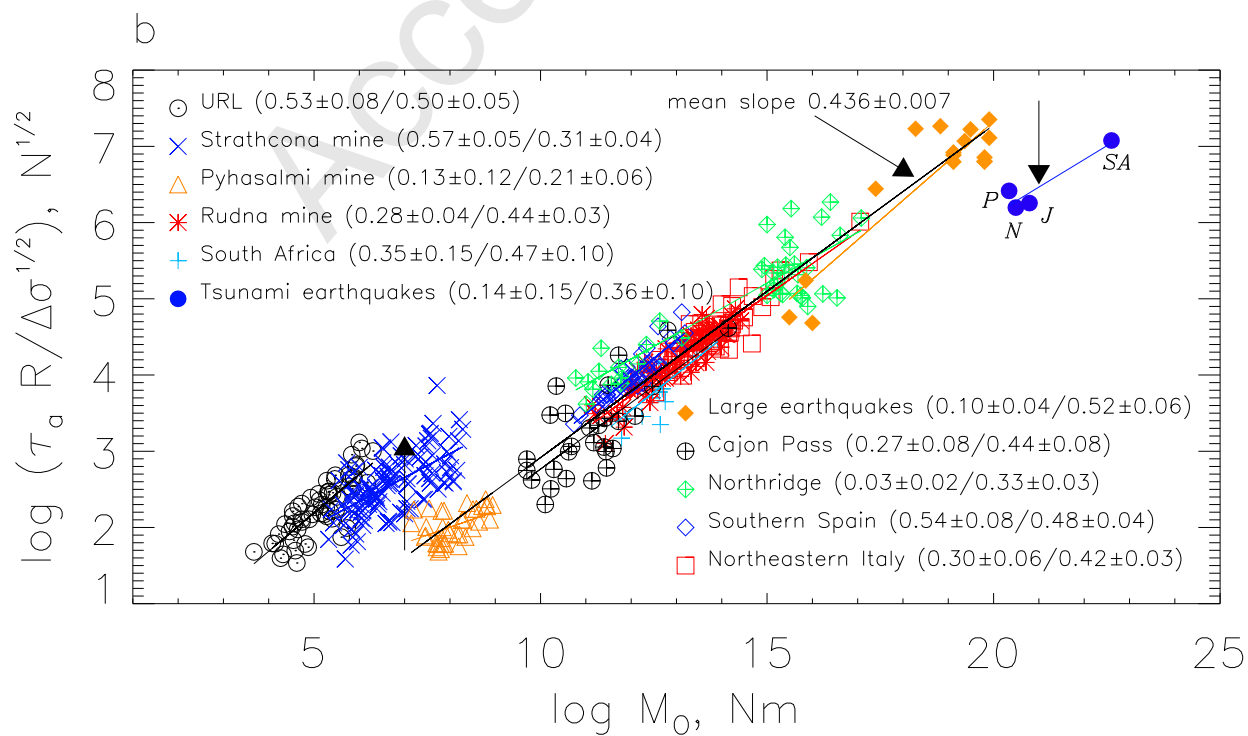
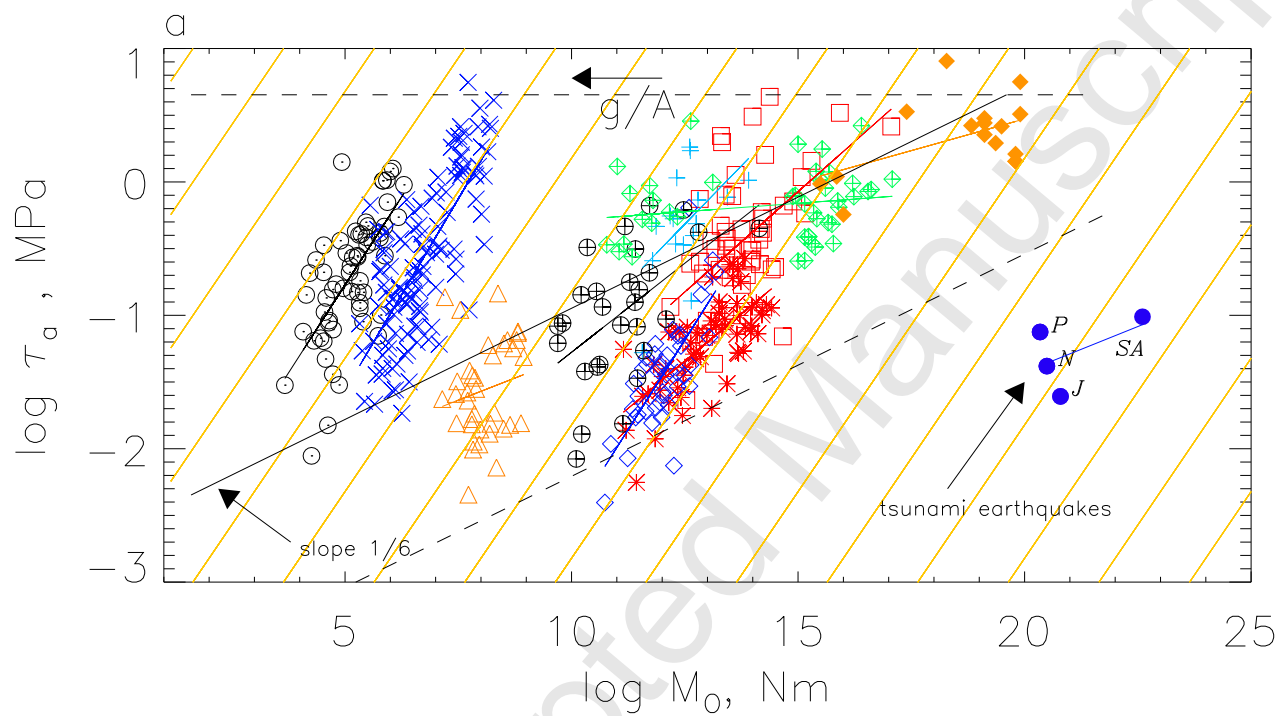
TABLES

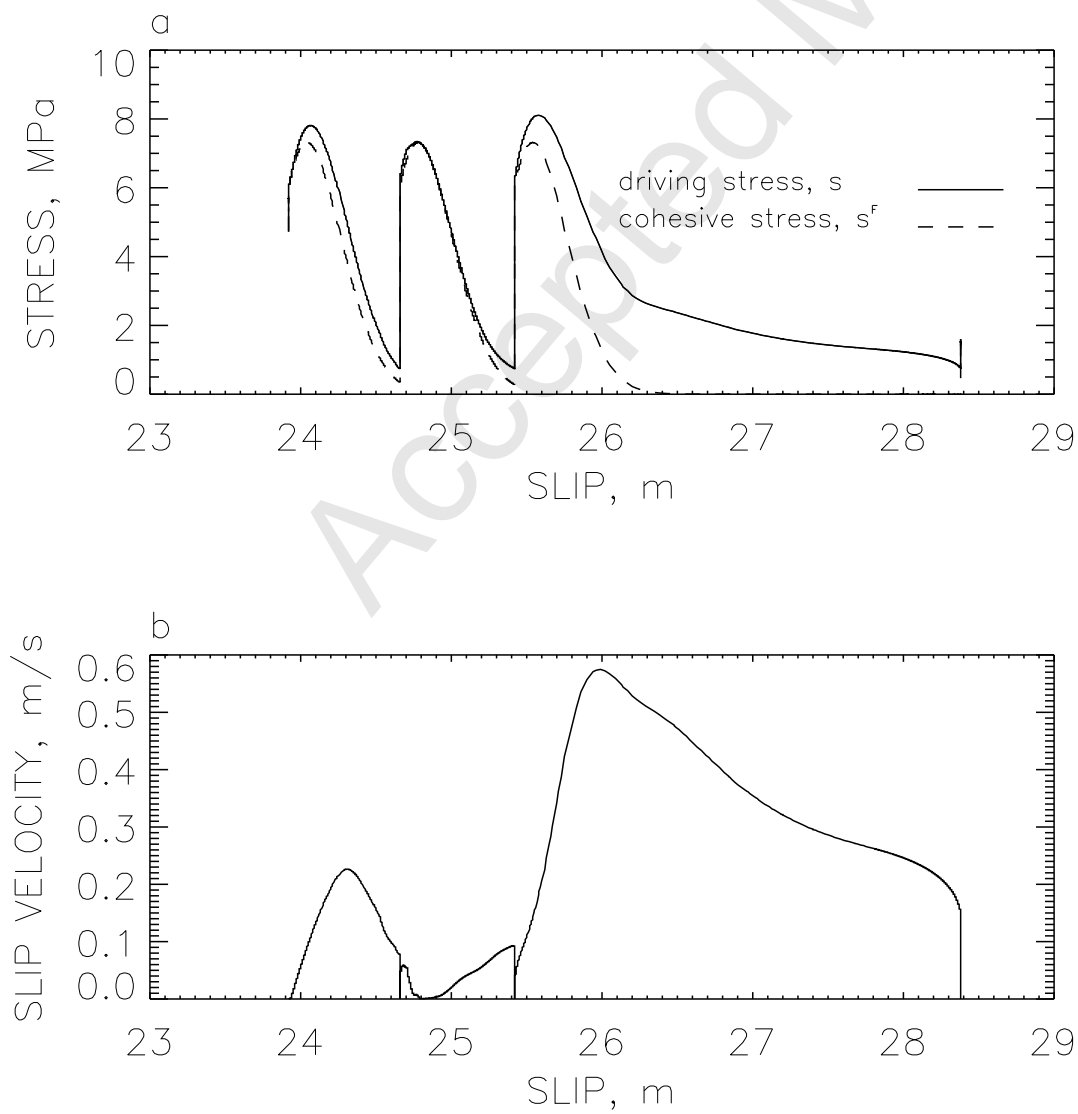
Table 1. Characteristics of earthquake populations illustrated in Fig.4.











Earthquake set parameters							
Earthquakes	Number of events	M_0 (N m)	R (m)	\bar{R} (m)	Slope 1/ correlation	Slope 2/ correlation	Reference
URL	60	$4.7e03 - 2.0e06$	0.25 – 1.0	0.6	$0.53 \pm 0.08/0.67$	$0.50 \pm 0.05/0.80$	Gibowicz <i>et al.</i> , 1991 ⁴
Strathona ¹	117	$2.1e05 - 1.9e08$	0.5 – 3.0	1.3	$0.57 \pm 0.05/0.75$	$0.31 \pm 0.04/0.63$	-
Strathona I	57	$4.9e05 - 1.9e08$	0.7 – 2.7	1.4	$0.65 \pm 0.07/0.79$	$0.50 \pm 0.07/0.73$	Urbancic and Young, 1993 ^{4,5}
Strathona II	60	$2.1e05 - 1.7e07$	0.5 – 3.0	1.3	$0.27 \pm 0.13/0.27$	$0.38 \pm 0.13/0.59$	Urbancic <i>et al.</i> , 2005 ^{4,5}
Pyhäsalmi	37	$1.4e07 - 8.8e08$	1.6 – 7.0	4.	$0.13 \pm 0.12/0.18$	$0.21 \pm 0.06/0.49$	Oye <i>et al.</i> , 1996 ⁵
Cajon Pass	28	$1.e09 - 1.e14$	6. – 220.	40.	$0.27 \pm 0.08/0.53$	$0.44 \pm 0.08/0.73$	Abercrombie and Rice, 2005
South Africa	16	$3.6e11 - 8.1e13$	24. – 120.	50.	$0.35 \pm 0.15/0.52$	$0.47 \pm 0.10/0.77$	McGarr, 1994 ⁵
Rudna	60	$1.4e11 - 2.6e13$	50. – 500.	230.	$0.28 \pm 0.04/0.70$	$0.44 \pm 0.03/0.91$	Gibowicz, 2007
South Spain	43	$1.e10 - 1.e14$	73. – 248.	134.	$0.54 \pm 0.08/0.74$	$0.48 \pm 0.04/0.91$	Garcia <i>et al.</i> , 2004 ⁵
Northeastern Italy	53	$1.e10 - 1.e14$	100. – 2700.	420.	$0.30 \pm 0.06/0.54$	$0.42 \pm 0.05/0.91$	Franceschina <i>et al.</i> , 2006 ⁵
Northridge ²	43	$1.e12 - 1.e17$	14. – 2544.	860.	$0.025 \pm 0.02/0.19$	$0.33 \pm 0.03/0.89$	-
Northridge afters.	29	$1.e14 - 1.e17$	492. – 2544.	864.	$0.17 \pm 0.08/0.38$	$0.21 \pm 0.13/0.30$	Abercrombie and Rice, 2005
Long Valley	14	$1.e10 - 1.e13$	14. – 89.	42.	$0.21 \pm 0.10/0.54$	$0.34 \pm 0.08/0.77$	Abercrombie and Rice, 2005
Large earthqs.	11	$1.e15 - 1.e20$	350. – 15.e03	9.e03	$0.10 \pm 0.04/0.51$	$0.52 \pm 0.06/0.91$	Abercrombie and Rice, 2005
Tsunami earthqs.	4	$3.1e20 - 4.e22$	$7.3e04 - 3.e05$	137.e03	$0.14 \pm 0.15/0.53$	$0.36 \pm 0.10/0.93$	see the main text
All events ³	296	$1.e07 - 1.e20$	1.6 – 15.e03	–	–	$0.436 \pm 0.007/0.97$	-

¹ combined Strathona I and Strathona II data.

² combined Northridge aftershocks and Long Valley data.

³ URL, Strathona, and tsunami data excluded.

⁴ The original data have been corrected to account for the finite bandwidth effects.

⁵ The original data have been recalculated from Brune to Madariaga model.